Low-temperature Ar/N_2 remote plasma nitridation of SiO_2 thin films

Amit Khandelwal[a)]
Department of Chemical Engineering, North Carolina State University, Raleigh, North Carolina 27695-7905

Hiro Niimi[b)]
Department of Physics, North Carolina State University, Raleigh, North Carolina 27695-8202

Gerald Lucovsky
Departments of Physics, Materials Science & Engineering, and Electrical & Computer Engineering, North Carolina State University, Raleigh, North Carolina 27695-8202

H. Henry Lamb[c)]
Department of Chemical Engineering, North Carolina State University, Raleigh, North Carolina 27695-7905

(Received 7 May 2002; accepted 19 August 2002)

Low-temperature nitridation of SiO_2 thin films by Ar/N_2 remote plasma processing was investigated using on-line Auger electron spectroscopy, angle-resolved x-ray photoelectron spectroscopy (ARXPS), and optical emission spectroscopy (OES). Nitridation experiments were performed at 300 °C using 30 W Ar/N_2 remote plasmas at 0.1 and 0.3 Torr. Ar/N_2 remote plasma exposure of 5 nm SiO_2 films for 30 min results in nitrogen incorporation throughout the films, independent of process pressure and plasma reactor configuration (i.e., upstream versus downstream N_2 injection). ARXPS indicates a $N-Si_3$ local bonding configuration with second nearest neighbor oxygen atoms. Ar/N_2 remote plasma exposure at 0.1 Torr results in higher nitrogen concentrations (8–10 at. %). Reactor configuration has a negligible effect at 0.1 Torr; conversely, downstream N_2 injection results in higher nitrogen concentrations (5–6 at. %) than upstream injection (3–4 at. %) at 0.3 Torr. OES indicates that the Ar/N_2 remote plasmas contain N_2 triplet excited states and ground-state N atoms. The Ar emission intensities and the saturation N concentrations in the resultant films follow similar trends with processing pressure and reactor configuration; the N_2 first positive emission intensities run counter to these trends. We infer that low-temperature SiO_2 nitridation by Ar/N_2 remote plasmas is a two-step process: O removal by Ar^+ ion bombardment and N insertion by plasma-generated active N species. Moreover, the first step appears to be rate limiting under the conditions employed in this study. Annealing the oxynitride films in N_2 at 900 °C decreases the N concentration and results in a more uniform nitrogen distribution. © *2002 American Vacuum Society.*
[DOI: 10.1116/1.1513635]

I. INTRODUCTION

Silicon dioxide (SiO_2) films have been used as the gate dielectric in metal–oxide–silicon (MOS) devices since the inception of integrated circuits; however, as device dimensions are aggressively scaled down into the sub-0.1 μm regime, the conventional SiO_2 gate dielectric faces a number of challenges. Ultrathin Si oxynitride (SiO_xN_y) films have been identified as leading candidates to replace conventional SiO_2 gate dielectrics for present and future ultralarge-scale-integrated circuits[1,2] due to their improved reliability[3–5] and boron penetration resistance.[6,7] Incorporation of N atoms at the top surface of the gate dielectric in $p+$ MOS field-effect transistors creates a barrier to boron penetration.[8,9] Nitrogen incorporation into SiO_2 increases the dielectric constant permitting the use of a physically thicker film which results in lower leakage currents.[10–12] Nitrogen incorporated near the $Si-SiO_2$ interface reduces hot-electron degradation and improves breakdown properties.[3,13–23] Recent industry trends suggest that a relatively uniform nitrogen concentration throughout the gate dielectric film may give optimum device performance.

A variety of processing techniques have been developed to form ultrathin Si oxynitride films at low temperatures. These include plasma processing,[19,24–27] low-pressure chemical vapor deposition,[28,29] jet vapor deposition,[30] low energy ion implantation,[31] (followed by oxidation) and atomic layer deposition.[32] Among these, remote plasma processing[33,34] offers unique capabilities for gate dielectric applications. Remote plasma processes for top surface nitridation of thermally grown oxides have been developed and applied in complementary MOS device applications.[24,35] We recently investigated nitridation of 3 nm SiO_2 films using He/N_2 remote plasmas.[36] By increasing the process pressure from 0.1 to 0.3 Torr, a relatively uniform nitrogen concentration profile was obtained within the resultant oxynitride film.

In this article, we report on the low-temperature nitrida-

a)Current address: Applied Materials, Inc., Santa Clara, CA 95054.
b)Current address: Texas Instruments, Inc., Dallas, TX 75265.
c)Author to whom correspondence should be addressed; electronic mail: lamb@eos.ncsu.edu

tion of 5 nm SiO_2 films using Ar/N_2 remote plasmas and the influence of postnitridation annealing at 900 °C on the nitrogen concentration profiles within the films. Nitridation experiments were performed at 300 °C using upstream and downstream Ar/N_2 remote plasma processes. In the upstream process, N_2 and Ar are excited in a remote rf discharge. In the downstream process, Ar atoms are excited in a remote rf plasma and N_2 is injected downstream. Nitridation experiments were performed at process pressures of 0.1 and 0.3 Torr to determine the effects of plasma confinement on the concentration and spatial distribution of nitrogen in the resultant oxynitride films. Angle-resolved x-ray photoelectron spectroscopy (ARXPS) was employed to determine the concentration, spatial distribution, and local chemical bonding of nitrogen in the films, and optical emission spectroscopy (OES) was used to provide an insight into the remote plasma chemistry.

II. EXPERIMENT

A. Apparatus

The nitridation experiments were performed using a remote plasma processing chamber that has been described previously.[37] The chamber has three main components; (i) radio frequency plasma tube (a quartz tube wrapped with a Cu coil to which 13.56 MHz radiation is applied), (ii) gas dispersal ring (for downstream gas injection without plasma excitation), and (iii) substrate heater stage. A Seiko–Seiki hybrid turbomolecular/drag pump is used for process pumping.

B. Materials and methods

The substrates were 50-mm-diam phosphorous-doped Si(100) with a resistivity of 5.0–10.0 Ω cm ($\sim 5\times 10^{15}$ cm^{-3}). After a conventional wet chemical cleaning, a 10-nm-thick sacrificial oxide was grown in a conventional thermal oxidation furnace at 900 °C, which was followed by a 20 min N_2 anneal at 900 °C to reduce suboxides at the $Si–SiO_2$ interface. The samples were then dipped in a dilute (1 wt. %) HF solution to completely remove the sacrificial oxide. Immediately following the HF dip, each sample was rinsed in de-ionized H_2O, blown dry with N_2, and loaded in the load-lock chamber of the processing tool.

The 5 nm SiO_2 films were formed by a three-step process involving remote plasma-enhanced chemical vapor deposition (RPECVD) and rapid thermal annealing (RTA). In the first step, Ar/O_2 remote plasma-assisted oxidation (RPAO) was used for $Si–SiO_2$ interface formation. In the second step, an upstream Ar/O_2 remote plasma with downstream injection of 2% SiH_4 in He was employed for SiO_2 RPECVD. The temperature, pressure, and rf power used for RPAO and RPECVD were 300 °C, 0.3 Torr, and 30 W, respectively. After RPECVD, the wafer was transferred into the RTA chamber under high vacuum, and then annealed at 900 °C for 30 s in 0.3 Torr He ambient (third step). The resultant SiO_2 films were nitrided at 300 °C using 30 W Ar/N_2 remote plasmas. Research-grade Ar and N_2 were metered at 160 and 60 sccm, respectively, using mass flow controllers. Nitridation experiments were performed at 0.1 and 0.3 Torr in the upstream and downstream configurations.

Postnitridation annealing at 900 °C in a N_2 ambient was performed in a conventional horizontal tube furnace with a quartz liner. The flow rate of research-grade N_2 during annealing was 5 slpm. The samples were inserted with the furnace idling at 200 °C, and the temperature was then ramped slowly to 900 °C. To test for thermal oxidation during annealing, a clean Si sample (with native oxide) was annealed in the furnace under similar conditions for 30 min. A negligible change in the native oxide thickness was observed.

C. Characterization

On-line Auger electron spectroscopy (AES) using a 3 keV primary electron beam was performed in an adjacent surface analysis chamber. AE spectra were collected in the $N(E)$ mode using a single-pass cylindrical mirror analyzer and differentiated numerically. $dN(E)/dE$ spectra were used to quantify the nitrogen concentrations at the top surface of the oxide using elemental sensitivity factors generated from Si, SiO_2, and Si_3N_4 standards.[38]

ARXP spectra were measured *ex situ* with a PHI 3057 x-ray photoelectron spectroscopy (XPS) system comprising a 10-360 spherical capacitor analyzer, Omni Focus III fixed-aperture lens, 16-element multichannel detector, and 257 DR11 PC interface card. The Mg anode of a PHI 1248 dual-anode (Mg/Al) x-ray source was used. The binding energies are referenced to the adventitious carbon peak at 284.8 eV. Film composition was determined using published elemental sensitivity factors.[39]

OES was used to monitor the electronically excited species in the Ar/N_2 remote plasmas. The plasma emission was sampled through a sapphire window and transmitted via optical fiber to an EG&G Princeton Applied Research Model 1235 triple-grating spectrograph and optical multichannel analyzer. The sapphire window was mounted on a mini-Conflat port located ~20 mm below the end of the plasma tube and ~15 mm above the gas-dispersal ring. A diffraction grating with 150 lines/mm, blazed at 650 nm, was used to collect spectra between 350 and 950 nm.

III. RESULTS

A. On-line AES

Figure 1 shows the temporal evolution of the surface N concentration (measured by on-line AES) of 5 nm SiO_2 films exposed to Ar/N_2 remote plasmas at 0.1 and 0.3 Torr. The surface N concentration initially increases with exposure time and then tends toward saturation. The data indicate that decreasing the process pressure from 0.3 to 0.1 Torr increases the saturation N concentration. The initial nitridation rate (initial slope of the plot in Fig. 1) is also greater at 0.1 Torr thus indicating faster nitridation kinetics at lower pressures. The data for upstream Ar/N_2 plasma nitridation were fit to the following pseudo-first order kinetic expressions:

$$0.1 \text{ Torr} \quad [\mathrm{N}] = 21.2\{1-\exp(-0.13t_N)\} \quad (\text{at. \%}), \quad (1)$$

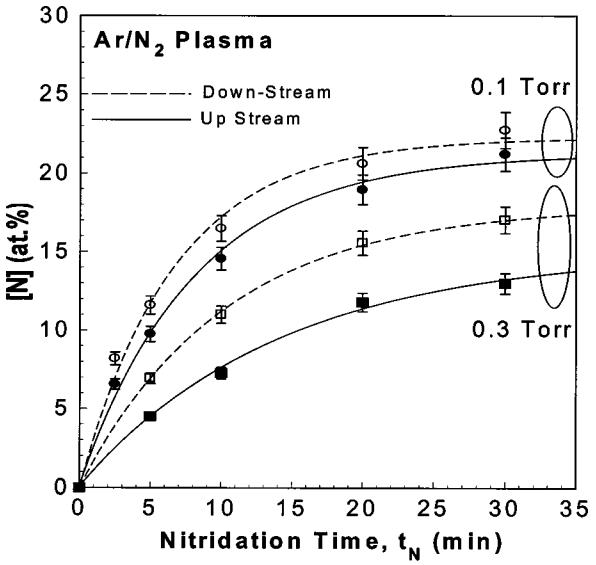

FIG. 1. Nitrogen concentration as a function of nitridation time, as determined by on-line AES, for 5 nm SiO_2 films exposed to 30 W Ar/N_2 remote plasmas at 0.1 and 0.3 Torr (upstream and downstream configurations). The substrate temperature was 300 °C in each experiment.

$$0.3\ \text{Torr} \qquad [\text{N}] = 15.1\{1-\exp(-0.10t_N)\} \quad (\text{at.}\,\%), \tag{2}$$

where t_N is the nitridation time. The saturation N concentration and first-order rate constant are ~40% and ~30% higher, respectively, for Ar/N_2 plasma nitridation at 0.1 Torr. Figure 1 also indicates that at each pressure, the nitridation rate and saturation N concentration are greater for downstream N_2 injection. The differences between upstream and downstream Ar/N_2 plasma nitridation are small at 0.1 Torr, but more pronounced when the pressure is increased to 0.3 Torr.

B. Angle-resolved XPS

Figure 2 shows the N 1*s* ARXP spectra of a 5 nm SiO_2 film following Ar/N_2 remote plasma exposure for 30 min at 30 W and 0.1 Torr in the upstream configuration. Spectra are shown for photoelectron take-off angles of 90°, 60°, 40°, 20°, and 10°. The take-off angle is defined as the angle between the sample surface and the analyzer axis (see Fig. 2 inset). A distinct N 1*s* peak is observed at 398.0±0.2 eV irrespective of take-off angle. This N 1*s* binding energy suggests a $N–Si_2$ (with a N dangling bond) or $N–Si_3$ bonding configuration. A strong N 1*s* signal is observed at a 10° take-off angle indicating the presence of nitrogen near the top surface of the film. As the take-off angle is increased, the XPS sampling depth increases enhancing the signals from the film and the Si substrate. The spectra in Fig. 2 evidence that increasing the take-off angle from 10° to 40° increases the N 1*s* signal indicating the presence of N within the film. A maximum in the N 1*s* signal is observed at ~40°, and the Si 2*p* (oxide, ~103 eV) signal also displays a maximum near 40° take-off angle. The XPS sampling depth is sufficiently

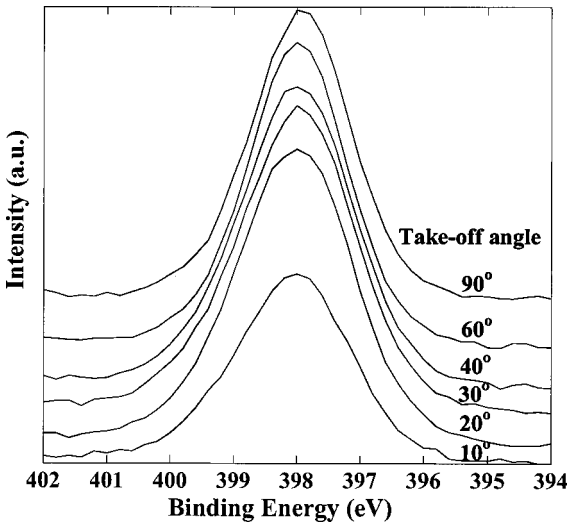

FIG. 2. N 1*s* photoelectron spectra at selected take-off angles for a 5 nm SiO_2 film after exposure to a 30 W Ar/N_2 remote plasma at 0.1 Torr (upstream) for 30 min.

large (>5 nm) at take-off angles greater than 40° that signal intensity from the oxynitride layer is reduced.

Figure 3 shows the normalized N 1*s*, O 1*s*, and Si 2*p* signals as a function of the sine of the take-off angle (which is proportional to sampling depth) for an SiO_2 film nitrided at 0.1 Torr (upstream) for 30 min. The signal intensities were normalized using the Si 2*p* (oxide) intensity at each angle, and each signal was then self-normalized at a take-off angle of 90°. The C 1*s* signal (not shown) decreases sharply with increasing sampling depth, consistent with the presence of adventitious carbon at the top surface. Conversely, the Si 2*p* (substrate) signal increases monotonically with increasing sampling depth. The trend of the N 1*s* signal with sampling depth is not similar to either the Si 2*p* (substrate) or C 1*s* signal, indicating that neither $Si–SiO_2$ interfacial nor SiO_2

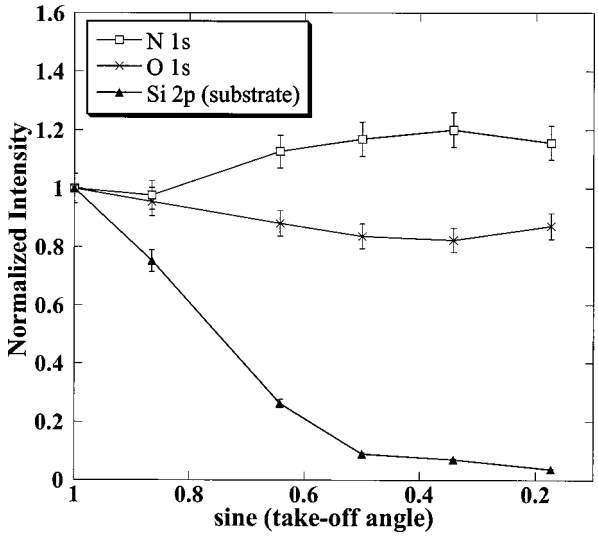

FIG. 3. Normalized N 1*s*, O 1*s*, and Si 2*p* (substrate) photoelectron signals as a function of the sine of the take-off angle. The 5 nm SiO_2 film was exposed to a 30 W Ar/N_2 remote plasma at 0.1 Torr (upstream) for 30 min.

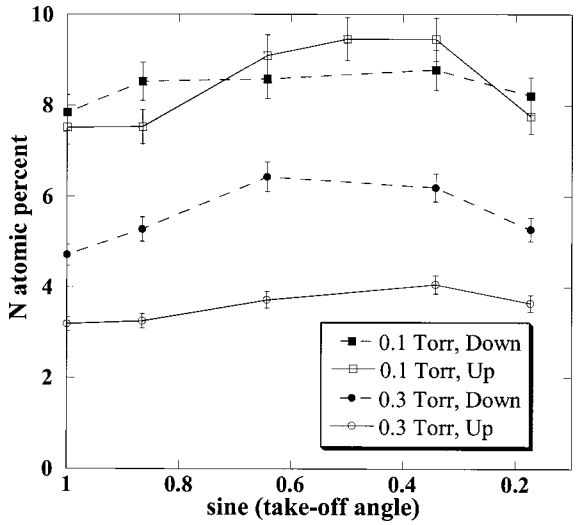

FIG. 4. Nitrogen concentration as a function ARXPS sampling depth for 5 nm SiO_2 films exposed to 30 W Ar/N_2 remote plasmas at 0.1 and 0.3 Torr (upstream and downstream configurations).

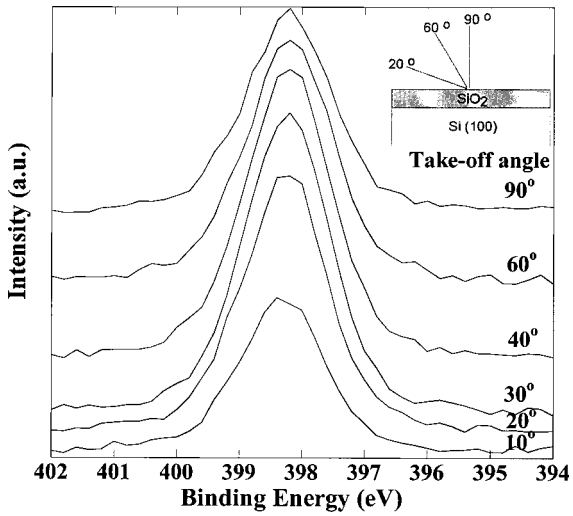

FIG. 5. N 1*s* photoelectron spectra at selected take-off angles for a 5 nm SiO_2 film after exposure to a 30 W Ar/N_2 remote plasma at 0.1 Torr (downstream) for 30 min and subsequent annealing in N_2 at 900 °C for 30 min.

top surface nitridation has occurred.[36,40] A maximum in the N 1*s* signal is observed at approximately 0.34 (a take-off angle of 20°); the O 1*s* signal exhibits a shallow minimum at the same position. Moreover, the N 1*s* and O 1*s* profiles are nearly mirror images of each other, which is consistent with substitution of N atoms for O atoms within the film.

Qualitatively similar ARXPS results were obtained for 5 nm SiO_2 films following Ar/N_2 remote plasma nitridation for 30 min, irrespective of process pressure and reactor configuration. A plot of N atomic percent versus the sine of the ARXPS take-off angle for samples nitrided for 30 min at 0.1 and 0.3 Torr and in the upstream and downstream configurations is shown in Fig. 4. The data indicate that the nitrogen concentration in the films increases as the pressure is reduced from 0.3 to 0.1 Torr. At 0.3 Torr, more nitrogen is incorporated in the downstream configuration; however, this effect is negligible at 0.1 Torr. The trends in N concentration with pressure and reactor configuration are similar to those observed by on-line AES (Fig. 1), but the absolute N concentrations measured by ARXPS are significantly lower than those estimated from the AE spectra.

Figure 5 shows the N 1*s* ARXP spectra of a 5 nm SiO_2 film nitrided using an Ar/N_2 remote plasma at 0.1 Torr (downstream), and then annealed in a N_2 ambient at 900 °C for 30 min. The Si 2*p* (substrate and oxide) signals do not indicate a change in film thickness, evidencing that no additional thermal oxidation/nitridation of the substrate occurred during annealing. A distinct N 1*s* peak is observed at 398.2 ±0.2 eV independent of take-off angle. The trend of the N 1*s* signal with take-off angle is similar to that before annealing; however, the N 1*s* intensity is reduced significantly. Figure 6 compares the normalized N 1*s*, O 1*s*, and Si 2*p* (substrate) intensities at selected take-off angles for the Si oxynitride film before and after annealing in N_2 at 900 °C for 30 min. The N 1*s* and the O 1*s* profiles are nearly mirror images both before and after the 30 min annealing step; however, there is less variation of the signals with sampling depth after annealing, suggesting a more uniform distribution of nitrogen in the oxynitride film.

Furnace annealing of SiO_2 films nitrided at 0.3 Torr (upstream and downstream) in a N_2 ambient at 900 °C gave similar results: a decrease in the amount of nitrogen after the annealing step and increased uniformity of the oxynitride films. Figure 7 shows the effect of N_2 annealing on the N atomic percent in the SiO_2 films nitrided at 0.1 Torr (downstream) and 0.3 Torr (upstream). The nitrogen concentration in the SiO_2 film nitrided at 0.1 Torr decreases from ~8 to ~4 at. % after annealing for 30 min and to ~2.5 at. % after annealing for an additional 30 min. A sample nitrided at 0.3 Torr (upstream) shows a decrease in the N concentration from ~3.5 to ~2.5 at. % after annealing for 30 min. Similar

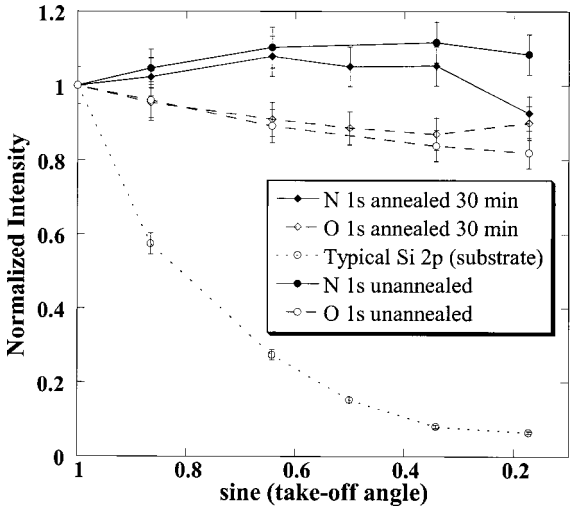

FIG. 6. Normalized N 1*s*, O 1*s*, and Si 2*p* (substrate) photoelectron signals as a function of the sine of the take-off angle. The 5 nm SiO_2 film was exposed to a 30 W Ar/N_2 remote plasma at 0.1 Torr (downstream) for 30 min and then annealed in N_2 at 900 °C for 30 min.

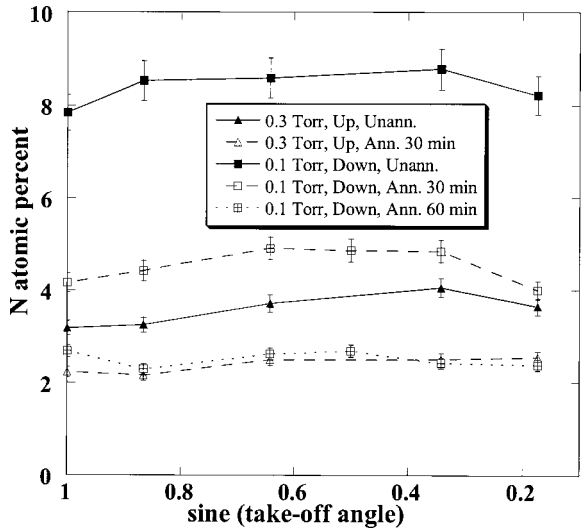

FIG. 7. Nitrogen concentration as a function of ARXPS sampling depth for 5 nm SiO_2 films after Ar/N_2 remote plasma exposure at 0.1 (downstream) and 0.3 Torr (upstream) for 30 min and subsequent annealing of the films in N_2 at 900 °C.

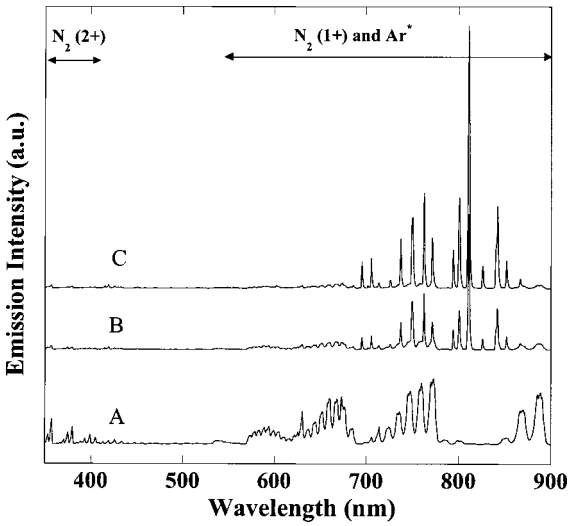

FIG. 9. OE spectra of 30 W N_2 and Ar/N_2 remote plasmas at 0.1 Torr: (a) undiluted N_2 (180 sccm) plasma, (b) Ar(160 sccm)/N_2(60 sccm) plasma (upstream), and (c) Ar(160 sccm)/N_2(60 sccm) plasma (downstream).

results were obtained for a sample nitrided at 0.3 Torr (downstream). The limiting N concentration after annealing appears to be ~2.5 at. %, irrespective of the initial N concentration. There is no indication of nitrogen accumulation at the $Si–SiO_2$ interface during annealing.

C. Optical emission spectroscopy

Figure 8 compares the OE spectra of Ar(160 sccm)/N_2(20 sccm) remote plasmas (upstream and downstream) and an N_2 remote plasma (180 sccm); in each case, the pressure and applied power were 0.3 Torr and 30 W, respectively. The N_2 first positive series (denoted "1+") appears in Fig. 8(a) as five bands of regularly spaced emission peaks in the visible and near infrared spectral regions. These bands arise from $B\,^3\Pi_g \rightarrow A\,^3\Sigma_u^+$ transitions. The strongest peaks of each 1+ band occur at 541, 594, 661, 773, and 889 nm. The relatively weak peaks that appear at 358, 380, 400, and 427 nm belong to the N_2 second positive series (denoted "2+"), which arises from $C^3\Pi_u \rightarrow B\,^3\Pi_g$ transitions. In addition to emission from excited N_2 molecules, numerous Ar emission lines (at 696.5, 750.4, 763.5, 772.4, 794.8, 800, 811.5, and 826.4 nm) are observed for Ar/N_2 remote plasmas. The N_2 1+ and 2+ emission bands of an upstream Ar/N_2 remote plasma at 0.3 Torr [Fig. 8(b)] are more intense than those of an N_2 remote plasma at 0.3 Torr [Fig. 8(a)]. The upstream configuration produces stronger N_2 1+ emission as compared to the downstream configuration [Fig. 8(c)]. Conversely, the Ar emission lines are more intense when N_2 is introduced downstream.

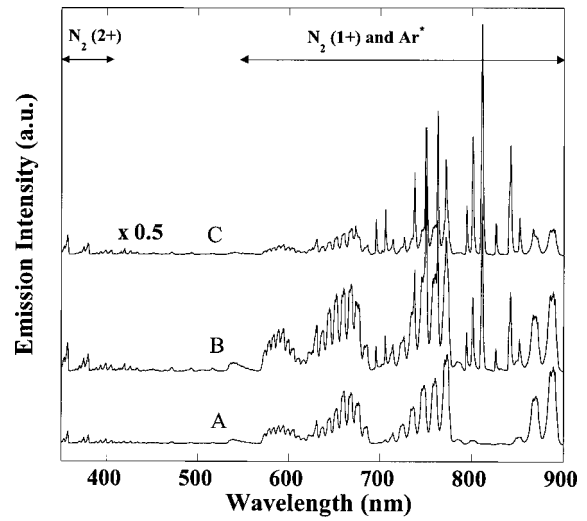

FIG. 8. OE spectra of 30 W N_2 and Ar/N_2 remote plasmas at 0.3 Torr: (a) undiluted N_2 (180 sccm) plasma, (b) Ar(160 sccm)/N_2(60 sccm) plasma (upstream), and (c) Ar(160 sccm)/N_2(60 sccm) plasma (downstream).

Figure 9 compares the OE spectra of Ar/N_2 plasmas (upstream and downstream) and a N_2 remote plasma operating at 0.1 Torr and 30 W. Stronger N_2 2+ emission (relative to 1+ emission) is observed from a N_2 remote plasma at 0.1 Torr [Fig. 9(a)] as compared to a N_2 remote plasma at 0.3 Torr [Fig. 8(a)]. The N_2 1+ and 2+ emission bands of the Ar/N_2 remote plasmas at 0.1 Torr [Figs. 9(b) and 9(c)] are much less intense than the Ar emission lines. Moreover, the N_2 1+ and 2+ emission intensities of the Ar/N_2 remote plasmas at 0.1 Torr are much less intense than those of a N_2 remote plasma at 0.1 Torr. The qualitative trends of the $N_2$1+ and Ar emission intensities with reactor configuration are, however, similar to those observed for Ar/N_2 remote plasmas at 0.3 Torr.

Emission from the first negative system of N_2^+ molecular ion transitions ($B\,^2\Sigma_u^+ \rightarrow X\,^2\Sigma_g^+$), which would include bands at 391.4 and 426.4 nm, was undetectable for Ar/N_2 and N_2 remote plasmas at 0.1 and 0.3 Torr. Moreover, emission from excited N atoms at 821.6 nm was undetectable for Ar/N_2 and N_2 plasmas at 0.1 and 0.3 Torr. Other N atom emission lines overlap the strong N_2 1+ emission bands.

IV. DISCUSSION

We recently reported that He dilution of N_2 remote plasmas significantly increases the nitridation rate of ultrathin SiO_2 films and the saturation N concentration in the resultant oxynitrides.[36] The results presented herein demonstrate that Ar dilution of N_2 remote plasmas produces similar effects. A 50 min exposure of a 3 nm SiO_2 film to a N_2 remote plasma at 0.1 Torr and 30 W incorporates only ~8 at. % N (as measured by on-line AES);[36] whereas, ~22 at. % N is incorporated by a 30 min Ar/N_2 plasma exposure at 0.1 Torr (Fig. 1). Changing the diluent from He to Ar at a process pressure of 0.1 Torr does not affect the nitridation rate or the saturation N concentration significantly; however, both are increased when Ar dilution is used at 0.3 Torr. He/N_2 and Ar/N_2 remote plasmas produce different N concentration profiles in the oxynitride films. Low-temperature nitridation of a 5 nm SiO_2 film using an Ar/N_2 remote plasma (at 0.1 or 0.3 Torr) yields a relatively uniform N concentration throughout the film. In contrast, nitridation of a 3 nm oxide using a He/N_2 remote plasma leads to top surface nitridation at 0.1 Torr and subsurface nitridation at 0.3 Torr.[36]

The Si oxynitride films produced by Ar/N_2 remote plasma exposure exhibit strong N 1*s* photoemission peaks at 398.0 ±0.2 eV binding energy. The N 1*s* binding energy for the $N–Si_3$ bonding configuration found in bulk Si_3N_4 is between 397.4 and 397.7 eV,[20,41,42] which is in reasonably close agreement with our results. $[(Si–)_2N–O]$ and other bonding configurations containing an N–O bond can be safely ruled out, since there is no evidence of a N 1*s* peak near 400 eV.[42] We attribute the slightly higher N 1*s* binding energy observed for the oxynitride films to an inductive effect of second nearest neighbor O atoms. Since O atoms are more electronegative than N atoms, replacement of N by O in second nearest neighbor positions will lead to a small positive binding energy shift. The magnitude of the shift will depend on the N concentration in the oxynitride film.

The saturation N concentrations determined by ARXPS are plotted for each combination of process pressure and Ar/N_2 remote plasma configuration (upstream versus downstream) in Fig. 10. Higher nitrogen concentrations are obtained at 0.1 Torr, irrespective of reactor configuration, and we have observed that the remote plasma is not confined to the plasma tube, but extends into the downstream processing chamber at this pressure. A significantly higher N concentration is achieved with downstream N_2 injection at 0.3 Torr; however, the effect of reactor configuration is negligible at 0.1 Torr. These observations are consistent with more complete mixing of upstream- and downstream-injected gases at lower pressure. The Ar emission intensities of Ar/N_2 remote plasmas and the saturation N concentrations in the resultant films follow similar trends, as illustrated in Fig. 10. In contrast, the N_2 1+ emission intensities of Ar/N_2 remote plasmas exhibit an opposing trend. The Ar emission intensity is proportional to the remote plasma density; whereas, the N_2 1+ emission intensity is proportional to the $N_2(B)$ concentration in the remote plasma.

We infer from OES that the Ar/N_2 and N_2 remote plasmas

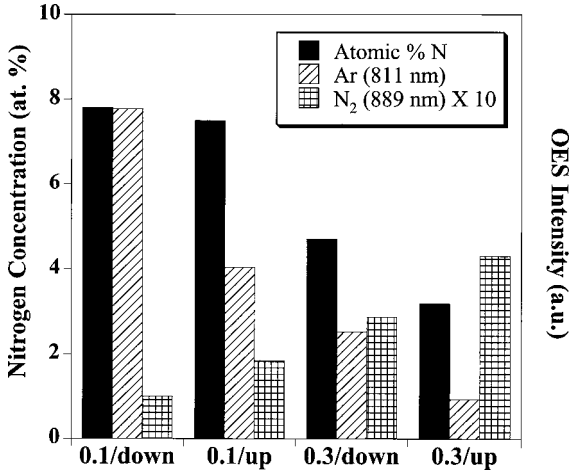

FIG. 10. Chart showing the saturation nitrogen concentrations (as measured by ARXPS) and the Ar (811 nm) and N_2 1+ (889 nm) OE intensities for different combinations of process pressure and Ar/N_2 remote plasma configuration.

contain N_2 triplet excited states and small, albeit potentially efficacious, concentrations of ^4S (ground state) and ^2D N atoms. The $N_2(C)$ and $N_2(B)$ triplet states, which have radiative lifetimes of 40 ns and ~6 μs, respectively, cascade to the $N_2(A)$ metastable state; hence the 2+ and 1+ emission intensities are good indicators of the $N_2(A)$ generation rate. Vibrationally excited $N_2(C)$ species produce N atoms via predissociation:[43]

$$N_2(C)(\nu>4)\rightarrow N(^4S)+N(^2D). \tag{3}$$

Consequently, the Ar/N_2 and N_2 remote plasmas may contain chemically significant concentrations of N atoms. Unfortunately, neither of these atomic N species can be detected directly by OES, since the $^2D\rightarrow{}^4S$ radiative transition is forbidden by dipole selection rules. The addition of Ar to a N_2 remote plasma at 0.3 Torr enhances the generation of $N_2(C)$ by excitation transfer.[44]

$$Ar^*+N_2(X)\rightarrow N_2(C)+Ar \tag{4}$$

as evidenced by the stronger 1+ and 2+ emission intensities in Fig. 8(b). A similar enhancement is not observed at 0.1 Torr, however, consistent with a lower collision frequency. Although a N_2 flow rate of 60 sccm (diluted in 160 sccm Ar at 30 W power) was used in the nitridation experiments and the OES measurements were made using 20 sccm N_2 (diluted in 160 scmm Ar at 30 W power), we have confirmed that the qualitative OES trends are unaffected by increasing the N_2 flow rate to 60 sccm.

The ARXPS intensity profiles in Fig. 3 suggest that nitridation occurs via replacement of O by N in the amorphous SiO_2 network. We infer that low-temperature nitridation by Ar/N_2 remote plasma exposure is a two-step process: O removal by Ar^+ ion bombardment and N insertion by plasma-generated active N species. The N incorporation pathway appears to be the same, independent of pressure and reactor configuration. Moreover, the first step appears to be rate limiting under the conditions employed in this study. This hy-

pothesis explains the similar dependencies of the saturation N concentrations and Ar emission intensities on process pressure and reactor configuration (Fig. 10). The very slow nitridation of SiO_2 using an N_2 remote plasma at 0.1 Torr (despite intense N_2 1+ emission) may be explained by the absence of Ar^+ (or significant N_2^+) ion bombardment. The observed enhancement of the nitridation rate at 0.3 Torr upon substituting Ar for He as the diluent adds further support for this hypothesis, since the lighter He^+ ions are expected to be relatively ineffective at removing O from the SiO_2 network. N_2^+ ions generated in He/N_2 remote plasmas, however, are capable of effecting the replacement of O by N in SiO_2 films. Specifically, we have attributed the top surface nitridation of SiO_2 films by He/N_2 remote plasma exposure at 0.1 Torr to N_2^+ species.[36] In contrast, the relatively uniform N concentration profile obtained by Ar/N_2 remote plasma processing at 0.1 Torr is attributed to an Ar^+ ion-assisted incorporation mechanism.

Annealing the oxynitride films at 900 °C in N_2 results in significant displacement of N by O[42] and a more uniform N concentration profile. The N 1*s* photoelectron binding energy after annealing (398.2±0.2 eV) indicates that the nitrogen remaining in the film retains the $N–Si_3$ bonding configuration. The displacement of nitrogen increases with annealing time, as illustrated in Fig. 7 using a sample prepared by Ar/N_2 remote plasma exposure at 0.1 Torr (downstream) and annealed twice at 900 °C for a total of 60 min. There appears to be a limiting N concentration of ~2.5 at. % that is independent of the initial N concentration achieved by low-temperature Ar/N_2 remote plasma processing. This was verified using a sample exposed to an Ar/N_2 remote plasma at 0.3 Torr (downstream) and annealed at 900 °C in N_2 for 30 min to achieve a uniform N concentration of ~2.5 at. %; there was no significant change in the N concentration profile on further annealing of this sample at 900 °C in N_2.

V. CONCLUSIONS

Argon dilution of N_2 remote plasmas significantly increases the nitridation rate of SiO_2 thin films and the saturation N concentration in the resultant oxynitrides. Low-temperature nitridation of 5 nm SiO_2 films using Ar/N_2 remote plasmas (at 0.1 and 0.3 Torr) produces oxynitrides with relatively uniform N concentration distributions. The oxynitride films exhibit strong N 1*s* photoemission peaks at 398.0±0.2 eV binding energy that are indicative of $N–Si_3$ local bonding with O second nearest neighbors. Higher N concentrations are obtained by Ar/N_2 remote plasma exposure at 0.1 Torr, independent of plasma reactor configuration (upstream versus downstream N_2 injection). The saturation N concentration obtained at 0.3 Torr is significantly higher when N_2 is injected downstream. We infer from OES that the Ar/N_2 remote plasmas contain N_2 triplet excited states and small, albeit potentially efficacious, concentrations of ^4S (ground state) and ^2D N atoms. The OES Ar emission intensities and the saturation N concentrations in the resultant films exhibit similar trends with process pressure and reactor configuration. In contrast, the N_2 1+ emission intensities of remote Ar/N_2 plasmas show an opposing trend. We infer that low-temperature SiO_2 nitridation by Ar/N_2 remote plasma exposure is a two-step process: O removal by Ar^+ ion bombardment and N insertion by plasma-generated active N species. Moreover, the first step appears to be rate limiting under the conditions employed in this study. Annealing the oxynitride films at 900 °C in N_2 decreases the N concentration and results in a more uniform nitrogen distribution.

ACKNOWLEDGMENTS

This work was supported in part by the SEMATECH/ Semiconductor Research Corporation Front End Processes Center and the Office of Naval Research.

[1]D. A. Buchanan and S. H. Lo, Microelectron. Eng. **36**, 13 (1997).
[2]T. Hori, S. Akamatsu, and Y. Odake, IEEE Trans. Electron Devices **39**, 118 (1992).
[3]T. Matsuoka, S. Taguchi, H. Ohtsuka, K. Taniguchi, C. Hamaguchi, S. Kakimoto, and K. Uda, IEEE Trans. Electron Devices **43**, 1364 (1996).
[4]M. Y. Hao, W. M. Chen, K. Lai, J. C. Lee, M. Gardner, and J. Fulford, Appl. Phys. Lett. **66**, 1126 (1995).
[5]Y. Okata, P. J. Tobin, P. Rushbrook, and W. L. DeHart, IEEE Trans. Electron Devices **41**, 191 (1994).
[6]K. S. Krisch, M. L. Green, F. H. Baumann, D. Brasen, L. C. Feldman, and L. Manchanda, IEEE Trans. Electron Devices **43**, 982 (1996).
[7]D. Mathiot, A. Straboni, E. Andre, and P. Debenest, J. Appl. Phys. **73**, 8215 (1993).
[8]G. Lucovsky, D. R. Lee, S. V. Hattangady, H. Niimi, Z. Jing, C. Parker, and J. R. Hauser, Jpn. J. Appl. Phys., Part 1 **34**, 6827 (1995).
[9]H. Niimi and G. Lucovsky, J. Vac. Sci. Technol. B **17**, 2610 (1999).
[10]H. Hwang, W. Ting, B. Maiti, D. Kwong, and J. Lee, Appl. Phys. Lett. **57**, 1010 (1990).
[11]E. C. Carr and R. A. Buhrman, Appl. Phys. Lett. **63**, 54 (1993).
[12]H. Fukuda, T. Arakawa, and S. Ohno, Jpn. J. Appl. Phys., Part 2 **29**, L2333 (1990).
[13]D. M. Fleetwood and N. M. Saks, J. Appl. Phys. **79**, 1583 (1996).
[14]T. Matsuoka, S. Taguchi, K. Taniguchi, C. Hamaguchi, C. Kakimoto, and J. Takagi, IEICE Trans. Electron. **E78-C**, 248 (1995).
[15]E. Cartier, D. A. Buchanan, and G. J. Dunn, Appl. Phys. Lett. **64**, 901 (1994).
[16]P. J. Tobin, Y. Okada, S. A. Ajuria, V. Lakhoita, W. A. Feil, and R. I. Hedge, J. Appl. Phys. **75**, 1811 (1994).
[17]Y. Okada, P. J. Tobin, and S. A. Ajuria, IEEE Trans. Electron Devices **41**, 1608 (1994).
[18]T. Hori, Microelectron. Eng. **22**, 245 (1993).
[19]D. Landheer, Y. Tao, D. X. Xu, G. I. Sproule, and D. A. Buchanan, J. Appl. Phys. **78**, 1818 (1995).
[20]M. Bhat, L. K. Han, D. Wristers, J. Yan, D. L. Kwong, and J. Fulford, Appl. Phys. Lett. **66**, 1225 (1995).
[21]R. I. Hedge, P. J. Tobin, K. G. Reid, B. Maiti, and S. A. Ajuria, Appl. Phys. Lett. **66**, 2882 (1995).
[22]K. S. Chang-Liao and L. C. Chen, Jpn. J. Appl. Phys., Part 2 **36**, L604 (1997).
[23]M. Alessandri, C. Clementi, B. Crivelli, G. Ghidini, F. Pellizzer, F. Martin, M. Imai, and H. Ikegawa, Microelectron. Eng. **36**, 211 (1997).
[24]S. V. Hattangady, H. Niimi, and G. Lucovsky, Appl. Phys. Lett. **66**, 3495 (1995).
[25]R. Kraft, T. P. Schneider, W. W. Dostalik, and S. V. Hattangady, J. Vac. Sci. Technol. B **15**, 967 (1997).
[26]H. Kobayashi, T. Mizokuro, Y. Nakato, K. Yoneda, and Y. Todokoro, Appl. Phys. Lett. **71**, 1978 (1997).
[27]S. V. Hattangady, H. Niimi, and G. Lucovsky, J. Vac. Sci. Technol. B **15**, 967 (1996).
[28]F. H. P. M. Habraken and A. E. T. Kuiper, Mater. Sci. Eng., R. **12**, 123 (1994).
[29]W. L. Hill, E. M. Vogel, V. Misra, P. K. McLarty, and J. J. Wortman, IEEE Trans. Electron Devices **43**, 15 (1996).
[30]T. P. Ma, Appl. Surf. Sci. **117/118**, 259 (1997).

[31]J. S. Pan, A. T. S. Wee, C. H. A. Huan, H. S. Tan, and K. L. Tan, Appl. Surf. Sci. **115**, 166 (1997).
[32]H. Goto, K. Shibahara, and S. Yokoyama, Appl. Phys. Lett. **68**, 3257 (1996).
[33]M. J. Helix, K. V. Vaidyanathan, B. G. Streetman, H. B. Dietrich, and P. K. Chatterjee, Thin Solid Films **55**, 143 (1978).
[34]G. Lucovsky, D. V. Tsu, R. A. Rudder, and R. J. Markunas, in *Thin Film Processes II* (Academic, San Diego, 1991).
[35]S. V. Hattangady, R. Kraft, D. T. Drider, M. A. Douglas, G. A. Brown, P. A. Tiner, J. W. Kuehne, P. E. Nicollian, and M. F. Pas, Tech. Dig. - Int. Electron Devices Meet., 495 (1996).
[36]H. Niimi, A. Khandelwal, H. H. Lamb, and G. Lucovsky, J. Appl. Phys. **91**, 48 (2002).
[37]H. Niimi and G. Lucovsky, J. Vac. Sci. Technol. A **17**, 3185 (1999).
[38]L. E. Davis, N. C. MacDonald, P. W. Palmberg, G. E. Riach, and R. E. Weber, *Handbook of Auguer Electron Spectroscopy: A Reference Book of Standard Data for Identification and Interpretation of Auguer Electron Spectroscopy Data* (Physical Electronics Industries, Inc., Eden Prairie, MN, 1987).
[39]J. F. Moulder, W. F. Stickle, P. E. Sobol, and K. D. Bomben, *Handbook of X-ray Photoelectron Spectroscopy: A Reference Book of Standard Spectra for Identification and Interpretation of XPS Data* (Physical Electronics Industries, Inc., Eden Prairie, MN, 1992).
[40]A. Khandelwal, B. C. Smith, and H. H. Lamb, J. Appl. Phys. **90**, 3100 (2001).
[41]J. L. Bischoff, F. Lutz, D. Bolmont, and L. Kubler, Surf. Sci. **251**, 170 (1991).
[42]S. K. Kaluri and D. W. Hess, J. Electrochem. Soc. **144**, 2200 (1997).
[43]A. N. Wright and C. A. Winkler, *Active Nitrogen* (Academic, New York, 1968).
[44]D. W. Setser, D. H. Stedeman, and J. A. Coxon, J. Chem. Phys. **53**, 1004 (1970).